Neutron electric dipole polarizability

Michael Engelhardt*
Department of Physics, New Mexico State University, Las Cruces, NM 88003, USA

Roman Höllwieser†
Department of Physics, University of Wuppertal, 42119 Wuppertal, Germany and
Department of Physics, New Mexico State University, Las Cruces, NM 88003, USA

Jesus Saenz‡
Institute of Engineering and Technology, Universidad Autónoma de Ciudad Juárez, 32310, Ciudad Juárez, Mexico and
Department of Physics, New Mexico State University, Las Cruces, NM 88003, USA

We revisit the neutron electric dipole polarizability and present results from a lattice calculation using the background method with increased statistics, taking into account connected as well as disconnected contributions. We further subtract the point-like contribution determined from a Foldy-Wouthuysen transformation in a preceding work.

Keywords: Neutron polarizabilities, neutron electric dipole polarizability, lattice QCD

I. INTRODUCTION

In [1], the general structure of the cross section in Compton scattering with polarized photons and nucleons is discussed. A low-energy expansion of the scattering amplitudes T_{if} leads to a cross section expression involving ten nucleon structure parameters, i.e., dipole, quadrupole, dispersion, and spin polarizabilities. In addition, $|T_{if}|^2$, are written in terms of invariant amplitudes T_i, which are decomposed into Born and non-Born contributions. Specifically, the spin-independent part of the non-Born contribution to the scattering amplitudes involve the coefficients α_E and β_M, i.e., respectively, the dipole electric and magnetic polarizabilities of the nucleon, which describe the magnitude of the electric and magnetic dipole moments induced on the nucleon by an applied electric field $\overrightarrow{E}$ or magnetic field $\overrightarrow{B}$[2].

As detailed in [3],the polarizabilities measure the response of the nucleon quark constituents to an applied electromagnetic field. The effective Hamiltonian of the interaction of a nucleon with an external electromagnetic field is written in terms of ten leading-order terms (in Gaussian units): [1]

$$\begin{aligned} H_{\text{eff}^{(2)}} = &-\frac{1}{2}(\alpha_E E^2 + \beta_M B^2 + \gamma_{E1}\sigma\cdot\left(E\times\dot{E}\right) \\ &+ \gamma_{M1}\sigma\cdot\left(B\times\dot{B}\right) - 2\gamma_{E2}E_{ij}\sigma_i B_j + 2\gamma_{M2}B_{ij}\sigma_i E_j \\ &+ \alpha_{E\nu}\dot{E}^2 + \beta_{M\nu}\dot{B}^2 + \frac{1}{6}\alpha_{E2}E_{ij}^2 + \frac{1}{6}\beta_{M2}B_{ij}^2 + \dots) \end{aligned} \tag{1}$$

where the quadrupole strengths of the electric and magnetic fields are

$$\begin{aligned} E_{ij} =& \frac{1}{2}\left(\nabla_i E_j + \nabla_j E_i\right) \\ B_{ij} =& \frac{1}{2}\left(\nabla_i B_j + \nabla_j B_i\right) \end{aligned} \tag{2}$$

* engel@nmsu.edu
† hoellwieser@uni-wuppertal.de
‡ jmsaenzv@nmsu.edu

[1] Polarizability units: In the SI system, there is an additional prefactor of 4π and the permittivity ε_0 and permeability μ_0 of the vacuum enter in the corresponding terms in the Hamiltonian.

and α_E and β_M are the electric and magnetic polarizabilities, γ_{E1}, γ_{M1}, γ_{E2}, and γ_{M2} are the spin polarizabilities, $\alpha_{E\nu}$, $\beta_{M\nu}$ are the dispersion polarizabilities, and α_{E2} and β_{M2} are the quadrupole polarizabilities [1, 4]. By writing the effective Hamiltonian in the form of Eq. (1), one assumes a sufficiently localized nucleon wave function in the sense that its energy depends on the local values of the electric and magnetic fields and their derivatives. This matter and the inherent limitations of Eq. (1) are discussed in more detail in [5].

Tripartite efforts are currently underway to determine the nucleon polarizabilities by experiments, analytically in Chiral Perturbation Theory (χPT), and by numerical calculation in lattice QCD.

In experimental results, the sum of the electric and magnetic polarizabilities is an integral of the total photoabsorption cross section in Compton scattering, i.e., the Baldin sum rule. Additional sum rules and recommended nucleon polarizability values based on experimental results are presented in [6]. The polarizability addends in the Baldin sum can be singled out by measuring the angular distribution of the photoabsorption in low-energy Compton scattering [2, 4]. For example, in [4], deuteron Compton scattering experimental data were fit to extract the electric and magnetic polarizability of the neutron. An alternative experimental method is presented in [6], the electric polarizability is measured in the scattering of slow neutrons in the presence of the electric field of a heavy nucleus, and results for the neutron polarizabilities are presented as the average of the individual results from deuteron Compton scattering and neutron electromagnetic scattering by the electric field of a lead nucleus. Phenomenological extraction of the dipole electric and magnetic, and spin polarizabilities are discussed in [7–28]. Dispersion relation analyses for experimental data of Compton scattering off protons or deuteron at low-energy (below pion production or near $\Delta(1232)$ resonance, for example) are discussed to extract nucleon structure constants such as the polarizabilities.

Chiral Perturbation Theory, a low-energy effective field theory of the strong interaction, provides a tool to explore low-energy hadronic physics, such as Compton Scattering off the nucleon, leading to the calculation of the nucleon electromagnetic polarizabilities in chiral theory [2, 29, 30].

Calculating hadron mass shifts in the presence of external electromagnetic fields in lattice QCD paves a way to calculate nucleon polarizabilities. Some of these efforts are recounted in [31–52]. Measurements on the lattice are performed on finite volumes and at unphysical (heavy) pion masses. The polarizabilities are given by the neutron mass shift in the presence of external static electric and magnetic fields, precisely on the part of the mass shift that is quadratic-in-the-fields. Chiral effective theory aims to connect lattice results to the pion mass and infinite volume physical limits [3, 9, 51, 53, 54]. As mentioned, the polarizability coefficients in Eq. (1) can be connected to the Compton scattering amplitudes in the low-energy limits. Matching the background field calculations of the polarizabilities in lattice QCD to the effective field theory description of the Compton amplitudes is explored amply in [55, 56], for example.

In this work, we focus on the lattice measurements of the electric polarizability α_E of the neutron. While other works on lattice hadron polarizability measurements have been performed in the quenched approximation [31–33, 57–61], in this work, we use a dynamical quark ensemble with a pion mass of 357 MeV, and improve the measurements of the electric polarizability of the neutron as compared to those reported in [35, 36] by considering connected and disconnected diagram contributions. In future work, we will present the lattice measurement of the spin electric polarizability γ_{E1}.

II. CALCULATION METHOD

This work improves the results of the neutron electric polarizability, which is obtained by the extraction of the hadron mass from the neutron two-point function in the presence of an external static electric field. The method has been applied successfully in [35, 36], but our work improves the neutron electric polarizability lattice measurements threefold; firstly, this work uses data sets with improved statistics, as compared to the previous calculations efforts in [35, 36]. Secondly, point neutron sinks are used. The former improvement in the data sets yield better statistical uncertainty in the correlators, while the latter avoids additional time dependencies related to smeared neutron sinks, which are discussed below and in [35]. Thirdly, the point-like contribution to the electric polarizability has been accounted for, i.e., the Foldy contribution, as presented in [5], has been subtracted from the lattice measurements, yielding a *bona fide* neutron polarizability.

The neutron two point function is the correlator

$$\langle N_\beta(y)\overline{N}_\alpha(x)\rangle = \frac{1}{Z}\int [DU][D\overline{\psi}][D\psi]\exp(-S[\psi,\overline{\psi},U])N_\beta(y)\overline{N}_\alpha(x) \tag{3}$$

where the action S, and the neutron fields $N, \overline{N}$ depend on the external electromagnetic field. After decomposing the action into one with vanishing external field plus one with the electromagnetic perturbation, i.e., $S = S_0 + S_E$, the correlator in Eq. (3) can be written in the form

$$\langle N_\beta(y)\overline{N}_\alpha(x)\rangle = \frac{\langle e^{-S_E}N_\beta(y)\overline{N}_\alpha(x)\rangle_0}{\langle e^{-S_E}\rangle_0} \tag{4}$$

that is, in terms of the averages in the absence of the external field. As mentioned in section I, the electric polarizability can be extracted from the quadratic-in-the-field part of the neutron mass. This translates to finding the aforementioned quadratic term in the Taylor expansion with respect to the applied electric field. The neutron two-point function becomes

$$\langle N_\beta(y)\overline{N}_\alpha(x)\rangle = \frac{\int [DU][D\psi][D\overline{\psi}]\exp(-S_0)(1 - S_E + S_E^2/2 + \dots)N_\beta(y)\overline{N}_\alpha(x)}{\int [DU][D\psi][D\overline{\psi}]\exp(-S_0)(1 - S_E + S_E^2/2 + \dots)} \tag{5}$$

The external electric field is taken in this work to point in the 3-direction, as described by Eq. (20), i.e., the gauge field is non-zero and linear in the electric field. In such a case, the external electric field modifies the gauge links as

$$U_3 \to \exp\left(iq\int dx_3 \cdot A_3\right)\cdot U_3 = (1 + iaqA_3 - a^2q^2A_3^2/2 + \dots)\cdot U_3 \tag{6}$$

where a is the lattice spacing and where q the quark fractional electric charge according to flavor. As explained in [36], after inserting Eq. (6) into the fermion action discretization of the Wilson type, two interaction vertices emerge, one linear in the external electric field while the other is quadratic; the coupling to the external electric field becomes

$$\begin{aligned} S_E = z_v\frac{1}{2}\sum_x \overline{\psi}(x)((iaqA_3 - a^2q^2A_3^2/2)\cdot U_3(x)\cdot(-1+\gamma_3)\cdot\psi(x+e_3) \\ + (iaqA_3 - a^2q^2A_3^2/2)\cdot U_3^\dagger(x-e_3)\cdot(1+\gamma_3)\cdot\psi(x-e_3)) \end{aligned} \tag{7}$$

where z_v is a renormalization factor that compensates the renormalization of the vertices in figure 1. The quark lines in these diagrams are populated by four-dimensional domain wall fields, and the coupling of said quark lines to the external field is attained via the current obtained from projecting the quark modes $\overline{\psi}$, ψ onto the domain walls [36]. As explained in [35], Wick's theorem yields the diagrammatic representation (c.f. figure 1) of the quadratic term in the Taylor expansion, with respect to the applied electric field, of the neutron two-point function. In the case of a time-independent Hamiltonian that depends on the electric

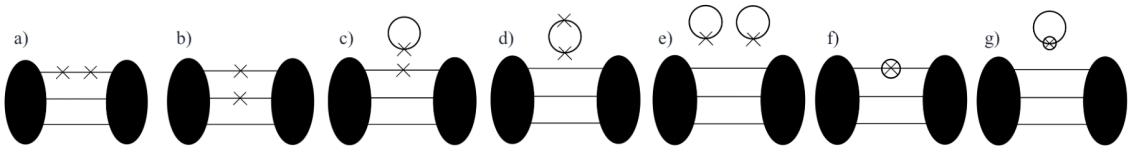

FIG. 1. Relevant diagram contributions to the neutron electric polarizability. Note that the crosses indicate the interaction vertices; linear in the external field interactions are represented with crosses, while the quadratic in the field interaction are represented by circles.

field E and gauge field A, which are considered to be two arbitrarily small parameters, projecting onto

unpolarized, zero-momentum neutrons, the two-point function exhibits an exponential behavior at a large time:

$$G(p=0,t)=\sum_{\vec{y}} Tr\left(\frac{1+\gamma_0}{2}\langle N(y)\overline{N}(x)\rangle\right) \overset{t\to\infty}{\longrightarrow} W\exp(-mt) \tag{8}$$

Expanding in A and E, the overlap between the neutron source and the ground state W, and the neutron mass m are written as

$$\begin{aligned} W &= W_0 + W^{(1)}(A,E) + W^{(2)}(A,E) + \cdots \\ m &= m_0 + m^{(2)}(A,E) + \cdots \end{aligned} \tag{9}$$

The second-order term in A and E in the neutron two-point function is written as

$$G^{(2)}(p=0,t) \overset{t\to\infty}{\longrightarrow} W_0\exp(-m_0 t)\left(\frac{W^{(2)}(A,E)}{W_0} - m^{(2)(A,E)t}\right) \tag{10}$$

and, thus, the neutron mass shift $m^{(2)}$ can be obtained from the temporal slope of the correlator ratio, defined as

$$R_2(t) = \frac{G^{(2)}(p=0,t)}{G^{(0)}(p=0,t)} \tag{11}$$

III. MEASUREMENT RESULTS

A. Quark renormalization

As discussed already in [35, 36], we need to renormalize our results. The renormalization factor $z_v = 3/Q$, where Q is a measurement of the number of valence quarks in the neutron, is deduced by measuring the three-point function without weighting by the quark electric charge q_f in the presence of an external gauge field of the form

$$A_o = \delta(x_0 - t) \tag{12}$$

for some time t between the hadron source and sink. The lattice regularization makes the number $Q = \int d^3x j_o$ deviate from 3, where j_0 is the temporal component of the quark current. One can obtain the number of quarks by averaging measurements of t at different lattice times. In this work, these measurements where taken at insertion times t in the interval $4a \leq t \leq 8a$, while the sink is introduced at $t_{\text{sink}} = 13a$. The uncertainties in both Q and $z_v = 3/Q$ were obtained by the jackknife method. As remarked in [36], light and strange quark lattice currents have different renormalization factors. To measure the aforementioned renormalization factors, the ratios Q_l, Q_s, respectively light and strange quarks, of the data with and without insertion should reach plateau values. The renormalization factors are then $3/Q_l$ and $3/Q_s$. Taking into account all diagrams in figure 1, every connected insertion is renormalized by the first value, but either renormalizes every loop insertion, e.g., a connected plus strange loop, or a mixed light-strange loop, is renormalized by a factor $9(Q_l Q_s)$. The charge renormalization factors for light and strange quarks on the $m_\pi = 357$ MeV ensemble were measured to be

$$Q_l = 2.629(20) \Rightarrow z_{v,l} = 1.1412(86) \tag{13}$$

$$Q_s = 2.7354(22) \Rightarrow z_{v,s} = 1.09671(89) \tag{14}$$

B. Foldy-Wouthuysen contribution to α_E at m_π= 357 MeV.

In order to extract the lattice measurement of the neutron's electric polarizability, one has to calculate the point-like contribution present in its energy spectrum. Such a a contribution to dipole electric polarizability

in long-know [62]. There are ten leading Foldy contributions for a zero-momentum neutron, which were determined from a Foldy-Wouthuysen transformation constructed in such a form as to yield the energy shift of a neutron in the presence of an external electromagnetic field. These contributions are reported in [5], and the Foldy-Wouthuysen electric polarizability contribution $\alpha_{\rm FW}$ is

$$\alpha_{\rm FW} = \frac{-\mu^2}{m_n} \tag{15}$$

where μ is the anomalous magnetic moment of the neutron and m_n is the neutron mass. Given that the lattice measurements of the electric polarizability are conducted at $m_\pi = 357$ MeV, the point-like contribution in Eq. (15) has to be evaluated at the pion mass scale. In [63], the isovector and isoscalar normalized anomalous magnetic moments are given by $\kappa_v^{\rm norm} = 2.518(57)$ and $\kappa_s^{\rm norm} = -0.030(22)$ in magnetons[2]. The neutron anomalous magnetic moment is given by

$$\kappa = \frac{\kappa_s^{\rm norm} - \kappa_v^{\rm norm}}{2} = -1.274(31) \tag{16}$$

As a function of the neutron mass m_n, the magnetic moment in GeV^{-1} is

$$\mu = \kappa \sqrt{\frac{1}{137}} \frac{1}{2m_n^{\rm phys}} \tag{17}$$

Evaluating 17 at the physical neutron mass $m_n^{\rm phys}$, as given in [64], the magnetic moment is then

$$\mu_{357\ \rm MeV} = -0.0579(14)\ \text{GeV}^{-1} \tag{18}$$

On the other hand, at $m_\pi = 355.98(80)$ MeV the neutron mass is $m_n = 1154.8(80)???$ MeV, as given in [65]. This mass value, along with the result given in 18, lead to a Foldy-Wouthuysen contribution (c.f. 15)

$$\alpha_{\rm FW}^{357\ \rm MeV} = (-0.2232 \pm 7.7 \times 10^{-7})\ 10^{-4}\ \text{fm}^{-3} error??? \tag{19}$$

As detailed in [5], Eq. (15) results from the energy shift of a poin-tlike neutron, so it must be subtracted from the α_E obtained from the lattice measurements described in this work.

C. Neutron mass shift

1. *Numerical measurements*

The numerical results discussed in this work are the result of the analysis of 448 gauge configurations generated with dynamical asqtad staggered quarks [66], provided by the MILC collaboration [67]. The lattice spacing $a = 0.124$ fm, with bare quark masses $am_l = 0.01$ and $am_s = 0.05$, which corresponds to a pion mass of 357 MeV. The quark lines of the diagrams in figure 1 that contribute to the neutron electric polarizability were populated with domain wall quarks, the disconnected contributions were estimated using complex $Z(2)$ stochastic sources. A technicality has been identified in [35]: a time-independent Hamiltonian ensures a stationary neutron wave function, while a time dependence is introduced by smeared neutron sinks, which would have to be addressed by considering additional contributions from additional diagrams to those shown in figure 1. In order to avoid these systematic effects we use point-like neutron sinks which are time-independent and invariant under gauge transformations of the external field. After first measurements we found the denominator of the correlator ratio $R_2(t)$ in Eq. (11) to be quite noisy, and therefore improved its statistics. For the results including disconnected diagrams in particular, the improved statistics however did not pay off and therefore we also quote the results of the original measurements.

[2] Note, in this work a pion mass of $m_\pi = 355$ MeV was given, which however corresponds to the same ensemble as the present one.

todo: describe electric field and 1 vs. 3 window fits...

A constant electric field is introduced in the 3-direction of the gauge field of the form

$$A_3 = E(t - t_0). \tag{20}$$

Different choices of time t_0 correspond to time shifts of the gauge component. Measurements at different t_0 allow one to treat the finite lattice effects, as the neutron energy spectrum depends on the gauge field A. It has been shown that there is a strong dependence of the nucleon polarizabilities on lattice volume, and it is claimed that a correction below 10% can be made. The finite volume corrections are found by studying the volume dependence of the values of polarizability obtained in calculations performed on lattices of different size [46]. The constant gauge field dominant effect is further elaborated in [35]. Furthermore, the present work used only one spatial lattice volume. Thus, to treat finite-size effects, polarizability measurements were performed at three different time values corresponding to three constant shifts of A_3. The polarizability measurements where made at $t_0 = -10a,\ 0,\ 6a$. These choices correspond to the three-window analysis, which probes the behavior of the correlation ratio R_2 at three times, thus defining the parabola of temporal slopes of the correlator ratio. In turn, the extremal slope corresponds, with a minus sign, to the mass shift of the neutron at the stationary point. In our work, the extremal slope was corrected for curvature effects; the need for such a correction arises from our fitting of linear functions, for a selected range of data points, to the cubic behavior of the correlator ratio, as will be discussed shortly.

The generic behavior of the correlator ratios in Eq. (11) is cubic as a function of time steps t/a. In our 3-window analysis, three values of the slope are obtained from a selected range of different data sets. These three slope values correspond to three points in a quadratic function, a parabola that results from the derivative of the cubic function that represents the generic behavior of the correlator ratios. Note that in each time window, a range of data has to be selected to obtain from it the slope. In our work, linear functions were fitted to the ranges of each of the data sets. This procedure yields slope, or points in a parabola, whose values deviate from the true values obtained from a cubic function. To define the correction to the minima, we defined a range M of data points, which is the difference between the final and initial time steps in the range. Assuming that a cubic function describes a set of perfect data points, we considered the sum of the squares of said perfect data point in a cubic function. By minimizing the sum, in turn, with respect to the slope p of the linear term and with respect to the constant term q of the linear function, an expression for p in terms of M and of the coefficients of the cubic function was obtained. The form of p is quadratic in time step s, say. The three values on the parabola were taken as the values of the slope at s= 21,11, 5. On the other hand, the exact minimum of a parabola is obtained in a straightforward calculation, starting from a function quadratic in time step t. By comparing the forms of the quadratic in s and quadratic in t functions, a correction Δp for the minimum of the parabola was found. Said correction has an interesting and useful feature; it is a constant that depends on the fitting range M. This means that the same correction may be applied to any and all time windows. The correction of the extremum was applied to the extracted minima of the fitted quadratic function.

The slopes presented in this work were obtained by performing χ^2 fits to the $R_2(t)$ data for a range of choice $5a \leq t \leq 7a$ in the three-window analysis, in which linear functions are fitted for the selected range at the three time windows of the cubic correlator ratio. As mentioned, the slopes obtained from these fits are three points in a quadratic function, which represents the derivative of the cubic function, for which the extremal value is determined. These extremal values were corrected for curvature of the fitted function, as justified above. This work also considers the fitting ranges $4a \leq t \leq 8a$ and $3a \leq t \leq 9a$ as alternatives.

2. *Electric polarizability α_E from connected diagrams in the 3-window analysis*

The static electric polarizability for the three fitting ranges are presented in table II with and without the Foldy-Wouthuysen contribution [5]. The electric polarizability measurements are consistent with those reported in [36].

Fit range $[t/a]$	5 to 7	4 to 8	3 to 9
Inflection point $[t/a]$	6.43(24)	6.7419)	7.28(13)
	6.27(27)	6.59(20)	7.15(14)
Extremal slope $[a^3]$	-0.0127(77)	-0.0149(58)	-0.0194(42)
	-0.0151(78)	-0.0154(59)	-0.0185(43)

TABLE I. Inflection points and extremal slopes of the χ^2 linear fits in the 3-window analysis with parabola minimum lift correction for connected diagrams. todo: results from reduced statistics are given in the lower lines

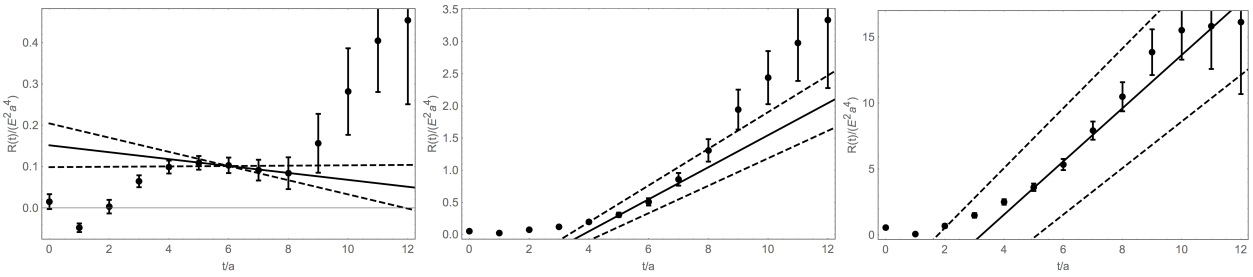

FIG. 2. Correlator ratio $R_2(t)$ and linear fits for the connected diagrams a), b), f), shown in Fig. 1, in units of E^2a^4. In these plots, the neutron source was placed at the fixed location $t = 0$, and the background field, c.f. 20, was varied with $t_0 = 6a$, $t_0 = 0$, $t_0 = -10a$ (from left to right). The dashed lines delimit the linear fit uncertainty in the slope.

Fit range $[t/a]$	5 to 7	4 to 8	3 to 9
α_E $[10^{-4}$ fm$^3]$	0.48(29)	0.57(22)	0.74(16)
	0.57(30)	0.59(22)	0.71(17)
$\alpha_E - \alpha_{FW}$ $[10^{-4}$ fm$^3]$	0.71(29)	0.79(22)	0.96(16)
	0.80(30)	0.81(22)	0.93(17)

TABLE II. Static electric polarizability α_E and reduced by the Foldy-Wouthuysen contribution $\alpha_E - \alpha_{FW}$ from the extremal slopes (connected diagrams, χ^2 fits) of the three fitting ranges in units of 10^{-4} fm^3. todo: results from reduced statistics are given in the lower lines

3. *Electric polarizability α_E, m_π=357 MeV measurements for connected diagrams in the 1-window analysis*

The 1-window analysis considers the $t_0 = 6a$ data. A cubic function is fitted, with and without a quadratic term, to assess the inflection point's shift. In contrast to the 3-window analysis discussed in III C 2, the range 5 to 7 provides only three points to be fitted, which may not be enough if they are to represent the cubic generic form of the correlator ratios, shown in figure 3. The data ranges from 4 to 8 and 3 to 9 were considered for the fit, with the latter the preferred range in the 1-window analysis.

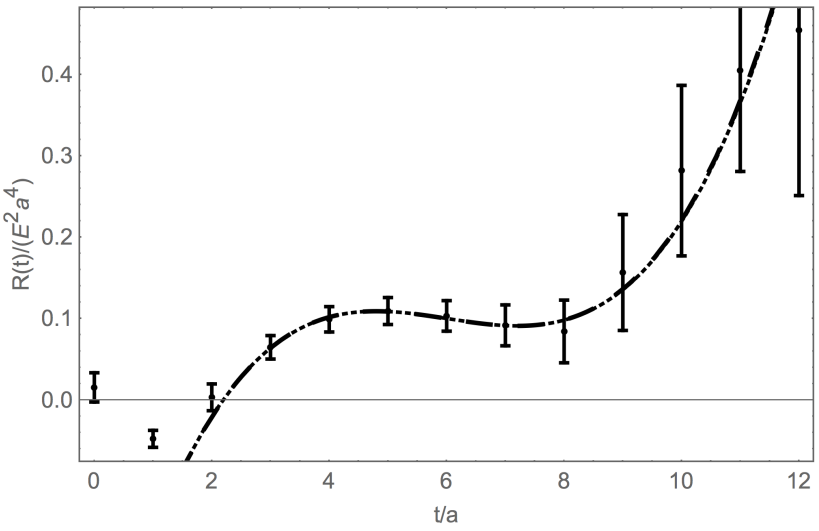

FIG. 3. Correlator ratio $R_2(t)$ for the connected diagrams a), b), f), shown in Figure 1, in units of E^2a^4. A cubic form was fitted with (dotted line) and without (dashed line) a quadratic term.

Table III shows the inflection points and extremal slopes. The inflection point positions are compatible with $t/a = 6$. The importance of the positions of these points becomes apparent in light of the possible retardation effects, which will be discussed below IV.

Fit range	4 to 8	3 to 9
Inflection point (t/a)	6.6(1.2) 6.55(89)	6.01(50) 6.06(45)
Extremal slope with a quadratic term $[a^3]$	-0.012(12) -0.016(11)	-0.0112(88) -0.0147(87)
Extremal slope w/o a quadratic term $[a^3]$	-0.012(10) -0.016(10)	-0.01123(95) -0.0150(93)

TABLE III. Inflection points and extremal slopes for the χ^2 cubic fits in the 1-window analysis for connected diagrams a), b), f), shown in Figure 1. todo: results from reduced statistics are given in the lower lines

The electric polarizability from the 1-window analysis is presented in Table IV. These measurements are consistent with those presented in Table II for the 3-window analysis of the data. Comparing these two result tables allows one to identify smaller statistical errors in the 3-window analysis than in the 1-window counterpart. However, it is not guaranteed that the correlator ratio $R_2(t)$ behaves in a purely cubic way, especially if scrutinized far away from the inflection point. In this regard, there is an unquantified systematic uncertainty in the 3-window analysis.

Fit range (t/a)	α [10^{-4} fm^3]	$\alpha - \alpha_{FW}$ [10^{-4} fm^3]
(with quadratic) 4 to 8	0.46(46)	0.69(46)
3 to 9	0.43(34)	0.65(36)
(without quadratic) 4 to 8	0.46(39)	0.68(39)
3 to 9	0.43(36)	0.65(36)

TABLE IV. Static electric polarizability α and reduced by the Foldy-Wouthuysen contribution $\alpha - \alpha_{FW}$ from the extremal slopes (1-window analysis, connected diagrams, χ^2 fits) of the two fitting ranges in units of 10^{-4} fm^3. todo: 'point' results?

4. *Electric polarizability α_E including all diagrams in the 3-window analysis*

The 3-window analysis was also performed for all diagrams, connected and disconnected, shown in 1. The correlator ratios $R_2(t)$ are shown in figure 11. The plots roughly correspond to the cubic behavior depicted in 5. The inflection points and extremal slopes were obtained for the fitting ranges 5 to 7, 4 to 8, 3 to 9, as shown in V.

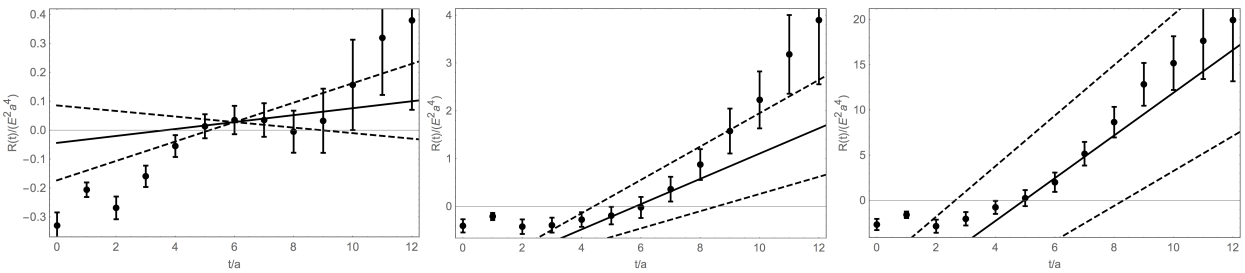

FIG. 4. Correlator ratio $R_2(t)$ for all diagrams shown in Figure 1, in units of E^2a^4. In these plots, the neutron source was placed at the fixed location $t = 0$, and the background field, c.f. 20, was varied with $t_0 = 6a$, $t_0 = 0$, $t_0 = -10a$ (from left to right).The dashed lines delimit the linear fit uncertainty in the slope.

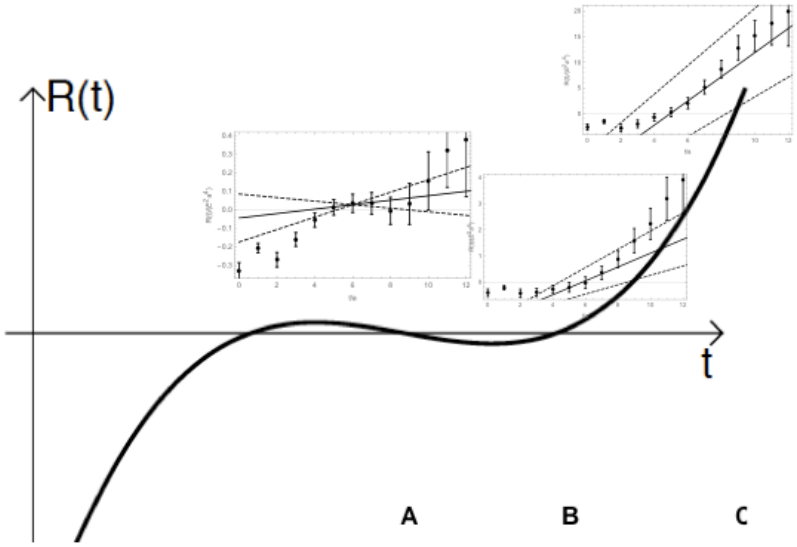

FIG. 5. 3-window generic cubic behavior for all diagrams. The plots in figure 11 are the three time windows shown here in their approximate positions.

Fit range $[t/a]$	5 to 7	4 to 8	3 to 9
Inflection point $[t/a]$	6.99(39)	6.97(38)	7.12(34)
	6.90(87)	7.12(91)	7.7(1.0)
Extremal slope $[a^3]$	-0.002(24)	0.001(19)	0.005(16)
	-0.006(61)	-0.023(50)	-0.037(46)

TABLE V. Inflection points and extremal slopes for the χ^2 linear fits in the 3-window analysis with parabola minimum lift correction, for all connected and disconnected diagrams. todo: results from reduced statistics are given in the lower lines

The electric polarizability for all diagrams was calculated from the results in table V for the selected fitting ranges, with and without the Foldy-Wouthuysen contribution. Table VI shows the electric polarizability measurements for the "multi point" dataset.

Fitting range (t/a)	5 to 7	4 to 8	3 to 9
α_E $[10^{-4}$ fm$^3]$	0.07(92)	-0.04(72)	0.19(72)
$\alpha_E - \alpha_{FW}$ $[10^{-4}$ fm$^3]$	0.29(92)	-0.19(63)	0.04(63)

TABLE VI. Static electric polarizability α_E and static electric polarizability minus Foldy-Wouthuysen contribution $\alpha_E - \alpha_{FW}$ from the extremal values (all diagrams, χ^2 fits, "multi point" dataset) of the three fitting ranges in units of 10^{-4} fm^3. todo: 'point' results?

5. *Electric polarizability α_E including all diagrams in the 1-window analysis*

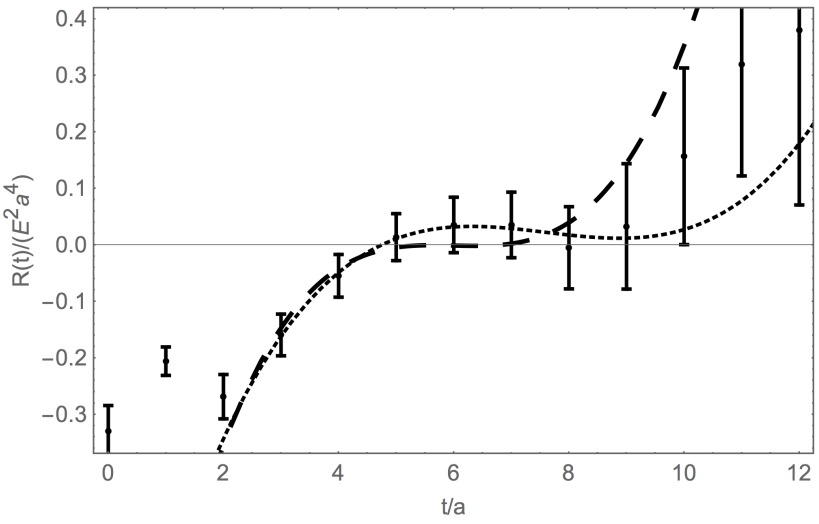

FIG. 6. Correlator ratio $R_2(t)$ for all diagrams (connected and disconnected) shown in Figure 1, in units of E^2a^4. A cubic form was fitted with (dotted line) and without (dashed line) a quadratic term.

Fit range $[t/a]$	4 to 8	3 to 9
Inflection point $[t/a]$	12(55)	7.6(2.0)
	6.4(2.0)	7(82)
Extremal slope with	-0.10(97)	-0.012(38)
a quadratic term $[a^3]$	0.012(60)	0.01(23)
Extremal slope w/o	-0.000(25)	-0.002(22)
a quadratic term $[a^3]$	0.011(60)	0.005(53)

TABLE VII. Inflection points and extremal slopes for the χ^2 cubic fits in the 1-window analysis for all connected and disconnected diagrams. todo: results from reduced statistics are given in the lower lines

	with quadratic term		w/o quadratic term	
Fit range $[t/a)]$	4 to 8	3 to 9	4 to 8	3 to 9
α_E $[10^{-4}$ fm$^3]$	4(37)	0.5(1.4)	0.01(94)	0.09(83)
$\alpha_E - \alpha_{FW}$ $[10^{-4}$ fm$^3]$	4(37)	0.7(1.4)	0.23(94)	0.31(83)

TABLE VIII. Static electric polarizability α and reduced by the Foldy-Wouthuysen contribution $\alpha - \alpha_{FW}$ from the extremal values (1-window analysis, connected and disconnected diagrams, χ^2 fits) of the two fit ranges in units of 10^{-4} fm^3. todo: point results?

IV. RETARDATION EFFECTS

In a time-independent Hamiltonian scenario, neutron excited states are present in the hadron source. These excited states decay and eventually only the ground state remains. This effect manifests in the three-point function; there is a plateau in the neutron energy. In our analysis, the Hamiltonian is time-dependent;

excited states come from the hadron source but are also continuously produced by the time evolution, i.e., a fast-changing electric field. This time dependence could be extracted from a time-dependent, expressed in Euclidean time, perturbation theory analysis. A fit function would contain the effects from excited states from the hadron source and the excited states generated by the electromagnetic perturbation, i.e., the time-varying electric field. Whereas in a time-independent Hamiltonian case there is no inflection point shift, in our time-dependent case, one of the indicators of the excited state presence is a consistent shift in the inflection point. However, we argue that there is no significant slope variation between $t = 6a$ and the inflection point in the three-window analysis. In the one-window analysis the shift in the inflection point is not resolvable. At the same time, the slope values at $t = 6a$ and at the shifted inflection point also agree within uncertainties. Thus, no excited state analysis is required for the results in our work.

A. Slope values at $t = 6a$ for the connected diagrams in the 3-window and 1-window analyses

Significant retardation effects would be suggested by non-negligible deviations of the slope at the shifted inflection point with respect to the slope at $t/a = 6$. Our results show compatible slope values at these points. Note that in our three- window analysis the fit of choice is $t/a = 5$ to 7, and the slopes agree within uncertainties even though the inflection points are shifted to the right, as shown in Figure 7.

Fit range $[t/a]$	5 to 7	4 to 8	3 to 9
Inflection point $[t/a]$	6.43(24)	6.74(19)	7.28(13)
Extremal slope $[a^3]$	-0.0127(77)	-0.0149(58)	-0.0194(42)
Slope at $t = 6a$ $[a^3]$	-0.0111(86)	-0.0109(68)	-0.0083(52)

TABLE IX. Inflection points, extremal slope and slope at $t = 6a$ for the χ^2 linear fits for connected diagrams in the 3-window analysis with parabola minimum lift correction.

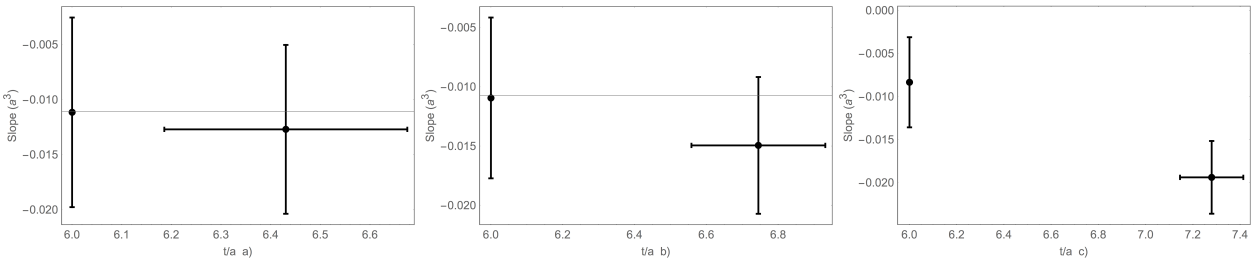

FIG. 7. Slope values at the shifted inflection points and at $t = 6a$ for the connected diagrams. a) 5 to 7, b) 4 to 8, c) 3 to 9 χ^2 fit ranges in the three-window analysis.

Our one-window analysis also confirms that an excited state analysis can be avoided; the values of the slopes at the points of inflection also agree within uncertainties. The results from table III are show in figure 8.

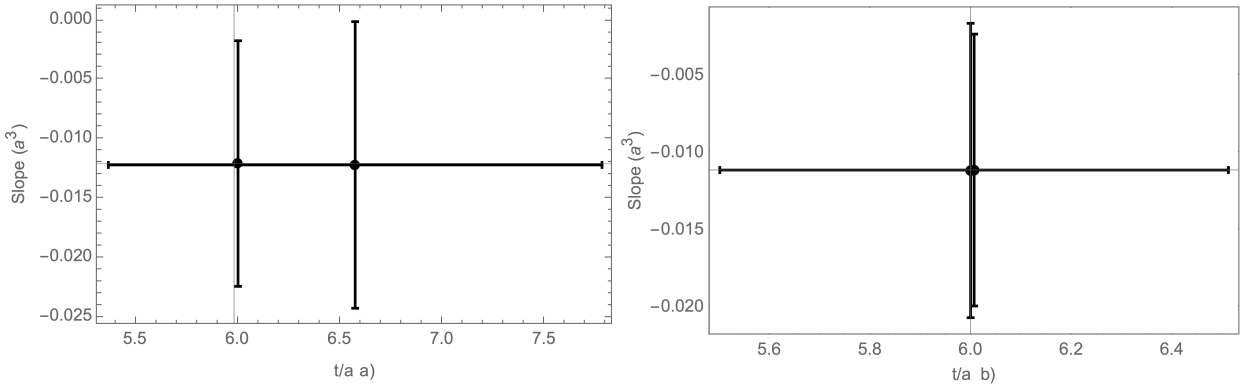

FIG. 8. Slope values for the χ^2 fits, with and without a quadratic term. a) 4 to 8, b) 3-9 fit ranges for the connected diagrams in the one-window analysis

B. Slope values at $t = 6a$ for all diagrams in the 3-window and 1-window analyses

The slope values at $t = 6a$ and at the shifted inflection point also agree within uncertainties, as shown in fiigure 9.

Fit range $[t/a]$	5 to 7	4 to 8	3 to 9
Inflection point $[t/a]$	6.99(39)	6.97(36)	7.12(34)
Extremal slope $[a^3]$	-0.002(24)	0.001(19)	0.005(16)
Slope at $t = 6a$ $[a^3]$	0.010(21)	0.010(16)	0.016(14)

TABLE X. Inflection points, extremal slope and slope at $t = 6a$ for the χ^2 linear fits for connected diagrams in the 3-window analysis with parabola minimum lift correction.

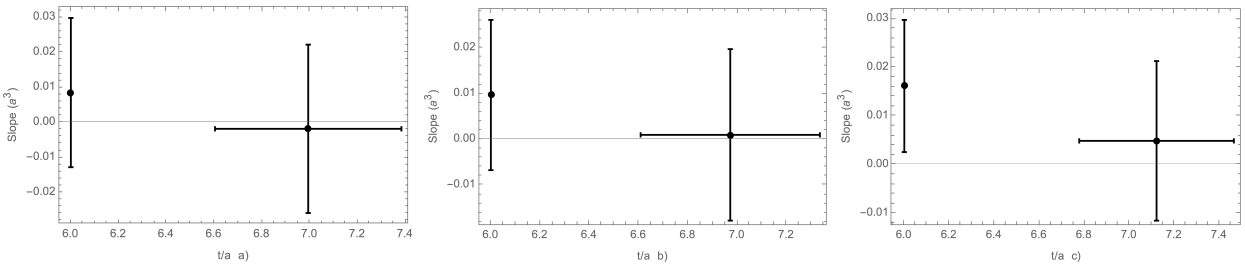

FIG. 9. Slope values at the shifted inflection points and at $t = 6a$ for all diagrams. a) 5 to 7, b) 4 to 8, c) 3 to 9 χ^2 fitting ranges in the three-window analysis.

In the χ^2 quadratic fits, in the one-window analysis, with and without a quadratic terms yield positions with a considerable uncertainty. However, the slopes at those points agree within uncertainties with those at the inflection point $t = 6a$, c.f. table III and figure 10.

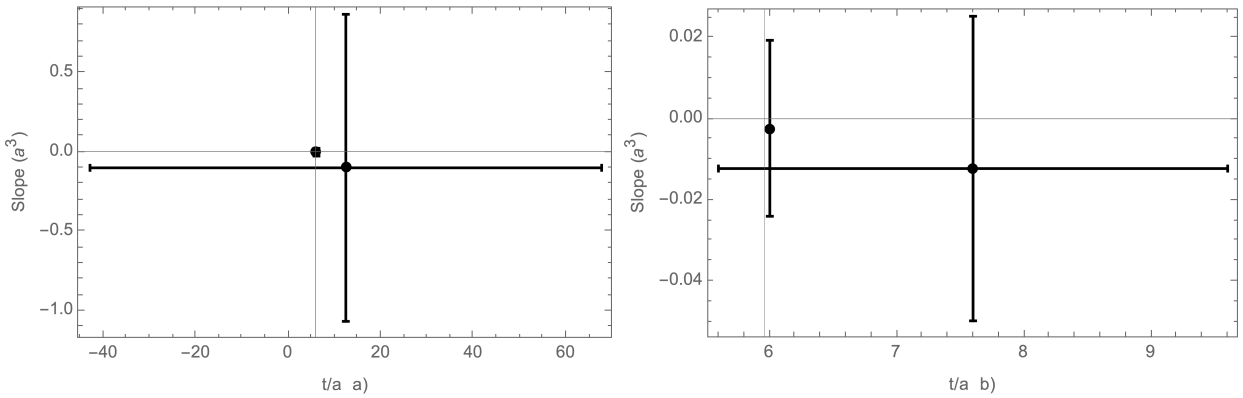

FIG. 10. Slope values extracted form the χ^2 fitting ranges a) 4 to 8 and b) 3 to 9 for all diagrams in the one-window analysis.

The previous connected and all diagrams results show slopes at the inflection point consistent with the slopes at $t = 6a$. Although the 3-window analysis shows that the inflection points shift, the one-window analyses yield large uncertainties in their positions. The slopes at theses points are also consistent with the ones at the inflection points of construction $t = 6a$. Consequently, we conclude that our results strongly suggest no excited-state analysis.

V. CONCLUSIONS

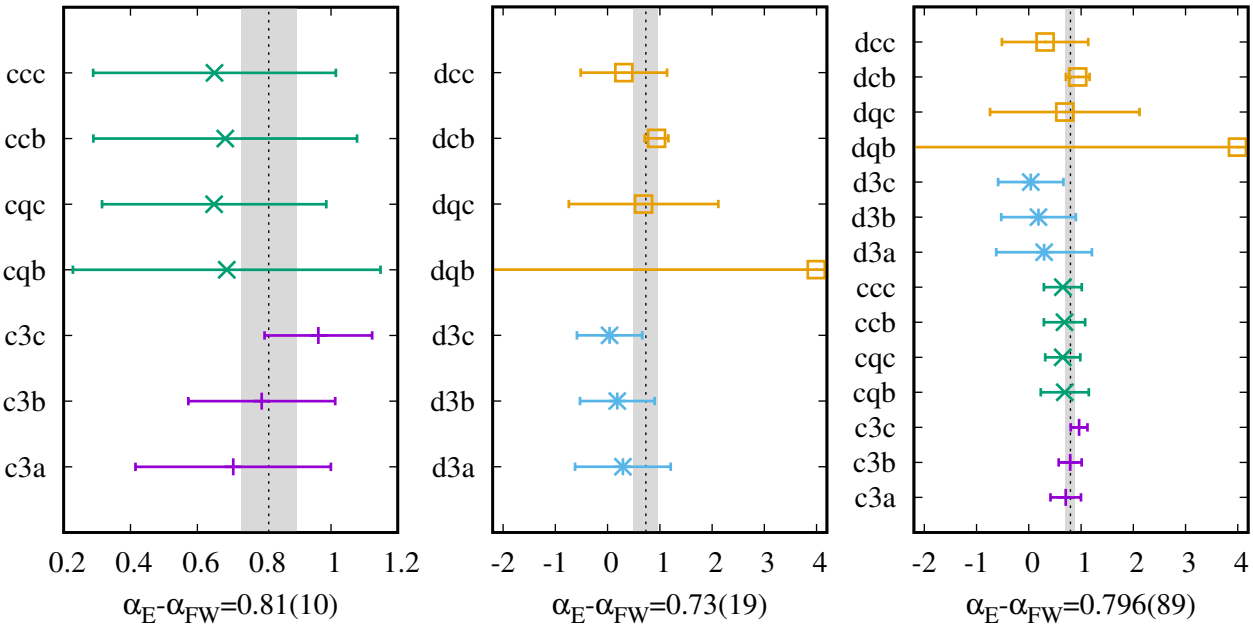

FIG. 11. Various fit results for the electric polarizability $\alpha_E - \alpha_{FW}$, 3-letter fit label: 1) connected (c) + disconnected (d) data; 2) 3-window fit (3), 1-window fit with (q) or without (c) quadratic term; 3) fit range 5 to 7 (a), 4 to 8 (b) and 3 to 9 (c) including corresponding (simple) averages in the abscissa labels (not taking into account correlations!).

ACKNOWLEDGMENTS

Fruitful discussions with S. A. Coon, W. Detmold, H. Grießhammer and B. Pasquini are acknowledged. This research was supported by the Erwin Schrödinger Fellowship program of the Austrian Science Fund FWF ("Fonds zur Förderung der wissenschaftlichen Forschung") under Contract No. J3425-N27 (R.H.) and the U.S. Department of Energy, Office of Science, Office of Nuclear Physics through grant DE-FG02-96ER40965 (M.E.,J.S.).

[1] D. Babusci, G. Giordano, A. I. L'vov, G. Matone, and A. M. Nathan, "Low-energy Compton scattering of polarized photons on polarized nucleons," *Phys. Rev. C* **58** (1998) 1013–1041, arXiv:hep-ph/9803347.

[2] F. Hagelstein, "Nucleon Polarizabilities and Compton Scattering as Playground for Chiral Perturbation Theory," *Symmetry* **12** no. 9, (2020) 1407, arXiv:2006.16124 [nucl-th].

[3] W. Detmold, B. C. Tiburzi, and A. Walker-Loud, "Electromagnetic and spin polarisabilities in lattice QCD," *Phys. Rev. D* **73** (2006) 114505, arXiv:hep-lat/0603026.

[4] M. I. Levchuk and A. I. L'vov, "Deuteron Compton scattering below pion photoproduction threshold," *Nucl. Phys. A* **674** (2000) 449–492, arXiv:nucl-th/9909066.

[5] J. Saenz, M. Engelhardt, and R. Höllwieser, "Energy of a pointlike neutron in an external electromagnetic field," *Phys. Rev. D* **104** no. 5, (2021) 056002, arXiv:2008.10691 [hep-ph].

[6] M. Schumacher, "Polarizability of the nucleon," *LHEP* **4** (2019) 4, arXiv:1907.05434 [hep-ph].

[7] B. R. Holstein, D. Drechsel, B. Pasquini, and M. Vanderhaeghen, "Higher order polarizabilities of the proton," *Phys. Rev. C* **61** (2000) 034316, arXiv:hep-ph/9910427.

[8] D. Drechsel, B. Pasquini, and M. Vanderhaeghen, "Dispersion relations in real and virtual Compton scattering," *Phys. Rept.* **378** (2003) 99–205, arXiv:hep-ph/0212124.

[9] R. P. Hildebrandt, H. W. Griesshammer, T. R. Hemmert, and B. Pasquini, "Signatures of chiral dynamics in low-energy compton scattering off the nucleon," *Eur. Phys. J. A* **20** (2004) 293–315, arXiv:nucl-th/0307070.

[10] M. Schumacher, "Polarizability of the nucleon and Compton scattering," *Prog. Part. Nucl. Phys.* **55** (2005) 567–646, arXiv:hep-ph/0501167.

[11] B. Pasquini, D. Drechsel, and M. Vanderhaeghen, "Proton spin polarizabilities from polarized Compton scattering," *Phys. Rev. C* **76** (2007) 015203, arXiv:0705.0282 [hep-ph].

[12] B. Pasquini, P. Pedroni, and D. Drechsel, "Higher order forward spin polarizability," *Phys. Lett. B* **687** (2010) 160–166, arXiv:1001.4230 [hep-ph].

[13] H. W. Griesshammer, J. A. McGovern, D. R. Phillips, and G. Feldman, "Using effective field theory to analyse low-energy Compton scattering data from protons and light nuclei," *Prog. Part. Nucl. Phys.* **67** (2012) 841–897, arXiv:1203.6834 [nucl-th].

[14] J. A. McGovern, D. R. Phillips, and H. W. Griesshammer, "Compton scattering from the proton in an effective field theory with explicit Delta degrees of freedom," *Eur. Phys. J. A* **49** (2013) 12, arXiv:1210.4104 [nucl-th].

[15] B. R. Holstein and S. Scherer, "Hadron Polarizabilities," *Ann. Rev. Nucl. Part. Sci.* **64** (2014) 51–81, arXiv:1401.0140 [hep-ph].

[16] **COMPTON@MAX-lab** Collaboration, L. S. Myers *et al.*, "Measurement of Compton Scattering from the Deuteron and an Improved Extraction of the Neutron Electromagnetic Polarizabilities," *Phys. Rev. Lett.* **113** no. 26, (2014) 262506, arXiv:1409.3705 [nucl-ex].

[17] **A2** Collaboration, P. P. Martel *et al.*, "Measurements of Double-Polarized Compton Scattering Asymmetries and Extraction of the Proton Spin Polarizabilities," *Phys. Rev. Lett.* **114** no. 11, (2015) 112501, arXiv:1408.1576 [nucl-ex].

[18] O. Gryniuk, F. Hagelstein, and V. Pascalutsa, "Evaluation of the forward Compton scattering off protons: Spin-independent amplitude," *Phys. Rev. D* **92** (2015) 074031, arXiv:1508.07952 [nucl-th].

[19] O. Gryniuk, F. Hagelstein, and V. Pascalutsa, "Evaluation of the forward Compton scattering off protons: II. Spin-dependent amplitude and observables," *Phys. Rev. D* **94** no. 3, (2016) 034043, arXiv:1604.00789 [nucl-th].

[20] F. Hagelstein, R. Miskimen, and V. Pascalutsa, "Nucleon Polarizabilities: from Compton Scattering to Hydrogen Atom," *Prog. Part. Nucl. Phys.* **88** (2016) 29–97, arXiv:1512.03765 [nucl-th].

[21] H. W. Griesshammer, J. A. McGovern, and D. R. Phillips, "Comprehensive Study of Observables in Compton Scattering on the Nucleon," *Eur. Phys. J. A* **54** no. 3, (2018) 37, arXiv:1711.11546 [nucl-th].

[22] B. Pasquini, P. Pedroni, and S. Sconfietti, "First extraction of the scalar proton dynamical polarizabilities from real Compton scattering data," *Phys. Rev. C* **98** no. 1, (2018) 015204, arXiv:1711.07401 [hep-ph].
[23] B. Pasquini and M. Vanderhaeghen, "Dispersion Theory in Electromagnetic Interactions," *Ann. Rev. Nucl. Part. Sci.* **68** (2018) 75–103, arXiv:1805.10482 [hep-ph].
[24] B. Pasquini, P. Pedroni, and S. Sconfietti, "Proton scalar dipole polarizabilities from real Compton scattering data, using fixed-t subtracted dispersion relations and the bootstrap method," *J. Phys. G* **46** no. 10, (2019) 104001, arXiv:1903.07952 [hep-ph].
[25] R. Miskimen, "Overview of the experimental achievements in nucleon and meson polarizabilites," *PoS* **CD2018** (2019) 015.
[26] **A2** Collaboration, P. P. Martel, "Compton Scattering and Hadron Polarizabilities," *PoS* **CD2018** (2019) 038.
[27] **A2** Collaboration, D. Paudyal *et al.*, "Extracting the spin polarizabilities of the proton by measurement of Compton double-polarization observables," *Phys. Rev. C* **102** no. 3, (2020) 035205, arXiv:1909.02032 [nucl-ex].
[28] J. A. Melendez, R. J. Furnstahl, H. W. Griesshammer, J. A. McGovern, D. R. Phillips, and M. T. Pratola, "Designing Optimal Experiments: An Application to Proton Compton Scattering," *Eur. Phys. J. A* **57** no. 3, (2021) 81, arXiv:2004.11307 [nucl-th].
[29] V. Bernard, N. Kaiser, and U. G. Meissner, "Chiral expansion of the nucleon's electromagnetic polarizabilities," *Phys. Rev. Lett.* **67** (1991) 1515–1518.
[30] V. Bernard, N. Kaiser, and U. G. Meissner, "Nucleons with chiral loops: Electromagnetic polarizabilities," *Nucl. Phys. B* **373** (1992) 346–370.
[31] H. R. Fiebig, W. Wilcox, and R. M. Woloshyn, "A Study of Hadron Electric Polarizability in Quenched Lattice QCD," *Nucl. Phys. B* **324** (1989) 47–66.
[32] J. C. Christensen, W. Wilcox, F. X. Lee, and L.-m. Zhou, "Electric polarizability of neutral hadrons from lattice QCD," *Phys. Rev. D* **72** (2005) 034503, arXiv:hep-lat/0408024.
[33] F. X. Lee, L. Zhou, W. Wilcox, and J. C. Christensen, "Magnetic polarizability of hadrons from lattice QCD in the background field method," *Phys. Rev. D* **73** (2006) 034503, arXiv:hep-lat/0509065.
[34] E. Shintani, S. Aoki, N. Ishizuka, K. Kanaya, Y. Kikukawa, Y. Kuramashi, M. Okawa, A. Ukawa, and T. Yoshie, "Neutron electric dipole moment with external electric field method in lattice QCD," *Phys. Rev. D* **75** (2007) 034507, arXiv:hep-lat/0611032.
[35] **LHPC** Collaboration, M. Engelhardt, "Neutron electric polarizability from unquenched lattice QCD using the background field approach," *Phys. Rev. D* **76** (2007) 114502, arXiv:0706.3919 [hep-lat].
[36] M. Engelhardt, "Progress Toward the Chiral Regime in Lattice QCD Calculations of the Neutron Electric Polarizability," *PoS* **LAT2009** (2009) 128, arXiv:1001.5044 [hep-lat].
[37] W. Detmold, B. C. Tiburzi, and A. Walker-Loud, "Extracting Electric Polarizabilities from Lattice QCD," *Phys. Rev. D* **79** (2009) 094505, arXiv:0904.1586 [hep-lat].
[38] W. Detmold, B. C. Tiburzi, and A. Walker-Loud, "Extracting Nucleon Magnetic Moments and Electric Polarizabilities from Lattice QCD in Background Electric Fields," *Phys. Rev. D* **81** (2010) 054502, arXiv:1001.1131 [hep-lat].
[39] M. Engelhardt, "Exploration of the electric spin polarizability of the neutron in lattice QCD," *PoS* **LATTICE2011** (2011) 153, arXiv:1111.3686 [hep-lat].
[40] A. Alexandru and F. X. Lee, "Neutron electric polarizability," *PoS* **LAT2009** (2009) 144, arXiv:0911.2520 [hep-lat].
[41] F. X. Lee and A. Alexandru, "Magnetic Moments of Negative-Parity Baryons from Lattice QCD," *PoS* **LATTICE2010** (2010) 148, arXiv:1011.4325 [hep-lat].
[42] F. X. Lee and A. Alexandru, "Spin Polarizabilities on the Lattice," *PoS* **LATTICE2011** (2011) 317, arXiv:1111.4425 [hep-lat].
[43] M. Lujan, A. Alexandru, W. Freeman, and F. Lee, "Electric polarizability of neutral hadrons from dynamical lattice QCD ensembles," *Phys. Rev. D* **89** no. 7, (2014) 074506, arXiv:1402.3025 [hep-lat].
[44] W. Freeman, A. Alexandru, M. Lujan, and F. X. Lee, "Sea quark contributions to the electric polarizability of hadrons," *Phys. Rev. D* **90** no. 5, (2014) 054507, arXiv:1407.2687 [hep-lat].
[45] E. V. Luschevskaya, O. E. Solovjeva, O. A. Kochetkov, and O. V. Teryaev, "Magnetic polarizabilities of light mesons in $SU(3)$ lattice gauge theory," *Nucl. Phys. B* **898** (2015) 627–643, arXiv:1411.4284 [hep-lat].
[46] M. Lujan, A. Alexandru, W. Freeman, and F. X. Lee, "Finite volume effects on the electric polarizability of neutral hadrons in lattice QCD," *Phys. Rev. D* **94** no. 7, (2016) 074506, arXiv:1606.07928 [hep-lat].
[47] T. Primer, W. Kamleh, D. Leinweber, and M. Burkardt, "Magnetic properties of the nucleon in a uniform background field," *Phys. Rev. D* **89** no. 3, (2014) 034508, arXiv:1307.1509 [hep-lat].
[48] R. Bignell, J. Hall, W. Kamleh, D. Leinweber, and M. Burkardt, "Neutron magnetic polarizability with Landau mode operators," *Phys. Rev. D* **98** no. 3, (2018) 034504, arXiv:1804.06574 [hep-lat].

[49] R. Bignell, W. Kamleh, and D. Leinweber, "Magnetic polarizability of the nucleon using a Laplacian mode projection," *Phys. Rev. D* **101** no. 9, (2020) 094502, arXiv:2002.07915 [hep-lat].
[50] R. Bignell, W. Kamleh, and D. Leinweber, "Pion magnetic polarisability using the background field method," *Phys. Lett. B* **811** (2020) 135853, arXiv:2005.10453 [hep-lat].
[51] F. He, D. B. Leinweber, A. W. Thomas, and P. Wang, "Chiral extrapolation of the magnetic polarizability of the neutral pion," *Phys. Rev. D* **102** no. 11, (2020) 114509, arXiv:2010.01580 [nucl-th].
[52] R. Bignell, W. Kamleh, and D. Leinweber, "Computing the magnetic field response of the proton," *EPJ Web Conf.* **245** (2020) 06033.
[53] V. Lensky, J. McGovern, and V. Pascalutsa, "Predictions of covariant chiral perturbation theory for nucleon polarisabilities and polarised Compton scattering," *Eur. Phys. J. C* **75** no. 12, (2015) 604, arXiv:1510.02794 [hep-ph].
[54] H. W. Griesshammer, J. A. McGovern, and D. R. Phillips, "Nucleon Polarisabilities at and Beyond Physical Pion Masses," *Eur. Phys. J. A* **52** no. 5, (2016) 139, arXiv:1511.01952 [nucl-th].
[55] J.-W. Lee and B. C. Tiburzi, "Background electromagnetic fields and nonrelativistic QED matching: Scalar case," *Phys. Rev. D* **89** no. 5, (2014) 054017, arXiv:1312.3969 [hep-ph].
[56] J.-W. Lee and B. C. Tiburzi, "Reconciling the lattice background field method with nonrelativistic QED: Spinor case," *Phys. Rev. D* **90** no. 7, (2014) 074036, arXiv:1407.8159 [hep-lat].
[57] W. Wilcox, "Lattice charge overlap. 2: Aspects of charged pion polarizability," *Annals Phys.* **255** (1997) 60–74, arXiv:hep-lat/9606019.
[58] W. Wilcox, "A Lattice investigation of the DMO sum rule," *Phys. Rev. D* **57** (1998) 6731–6740, arXiv:hep-lat/9803013.
[59] L. Zhou, F. X. Lee, W. Wilcox, and J. C. Christensen, "Magnetic polarizability of hadrons from lattice QCD," *Nucl. Phys. B Proc. Suppl.* **119** (2003) 272–274, arXiv:hep-lat/0209128.
[60] J. C. Christensen, F. X. Lee, W. Wilcox, and L.-m. Zhou, "Electric polarizability of hadrons," *Nucl. Phys. B Proc. Suppl.* **119** (2003) 269–271, arXiv:hep-lat/0209043.
[61] F. Lee, L.-M. Zhou, W. Wilcox, and J. Christensen, "Magnetic polarizability of hadrons in the background field method," *PoS* **LAT2005** (2006) 031.
[62] L. L. Foldy, "Electric Polarizability of the Neutron," *Phys. Rev. Lett.* **3** (1959) 105–105.
[63] J. R. Green, M. Engelhardt, N. Hasan, S. Krieg, S. Meinel, J. W. Negele, A. V. Pochinsky, and S. N. Syritsyn, "Excited-state effects in nucleon structure on the lattice using hybrid interpolators," *Phys. Rev. D* **100** no. 7, (2019) 074510, arXiv:1907.11950 [hep-lat].
[64] **Particle Data Group** Collaboration, C. Patrignani *et al.*, "Review of Particle Physics," *Chin. Phys. C* **40** no. 10, (2016) 100001.
[65] **LHPC** Collaboration, J. D. Bratt *et al.*, "Nucleon structure from mixed action calculations using 2+1 flavors of asqtad sea and domain wall valence fermions," *Phys. Rev. D* **82** (2010) 094502, arXiv:1001.3620 [hep-lat].
[66] G. P. Lepage, "Flavor symmetry restoration and Symanzik improvement for staggered quarks," *Phys. Rev. D* **59** (1999) 074502, arXiv:hep-lat/9809157.
[67] C. W. Bernard, T. Burch, K. Orginos, D. Toussaint, T. A. DeGrand, C. E. Detar, S. Datta, S. A. Gottlieb, U. M. Heller, and R. Sugar, "The QCD spectrum with three quark flavors," *Phys. Rev. D* **64** (2001) 054506, arXiv:hep-lat/0104002.